Journal of Optics

ACCEPTED MANUSCRIPT • OPEN ACCESS

Microdroplet-tin plasma sources of EUV radiation driven by solid-state-lasers (Topical Review)

To cite this article before publication: Oscar Versolato *et al* 2022 *J. Opt.* in press https://doi.org/10.1088/2040-8986/ac5a7e

Manuscript version: Accepted Manuscript

Accepted Manuscript is "the version of the article accepted for publication including all changes made as a result of the peer review process, and which may also include the addition to the article by IOP Publishing of a header, an article ID, a cover sheet and/or an 'Accepted Manuscript' watermark, but excluding any other editing, typesetting or other changes made by IOP Publishing and/or its licensors"

This Accepted Manuscript is **© 2022 The Author(s). Published by IOP Publishing Ltd.**.

As the Version of Record of this article is going to be / has been published on a gold open access basis under a CC BY 3.0 licence, this Accepted Manuscript is available for reuse under a CC BY 3.0 licence immediately.

Everyone is permitted to use all or part of the original content in this article, provided that they adhere to all the terms of the licence https://creativecommons.org/licences/by/3.0

Although reasonable endeavours have been taken to obtain all necessary permissions from third parties to include their copyrighted content within this article, their full citation and copyright line may not be present in this Accepted Manuscript version. Before using any content from this article, please refer to the Version of Record on IOPscience once published for full citation and copyright details, as permissions may be required. All third party content is fully copyright protected and is not published on a gold open access basis under a CC BY licence, unless that is specifically stated in the figure caption in the Version of Record.

View the article online for updates and enhancements.

This content was downloaded from IP address 192.87.153.12 on 31/03/2022 at 10:55

Microdroplet-tin plasma sources of EUV radiation driven by solid-state-lasers (Topical Review)

O. O. Versolato,[1, 2, *] J. Sheil,[1, 2] S. Witte,[1, 2] W. Ubachs,[1, 2] and R. Hoekstra[1, 3]
[1]*Advanced Research Center for Nanolithography (ARCNL),*
Science Park 106, 1098 XG Amsterdam, The Netherlands
[2]*Department of Physics and Astronomy, and LaserLaB, Vrije Universiteit Amsterdam,*
De Boelelaan 1081, 1081 HV Amsterdam, The Netherlands.
[3]*Zernike Institute for Advanced Materials, University of Groningen,*
Nijenborgh 4, 9747 AG Groningen, The Netherlands

Plasma produced from molten-tin microdroplets generates extreme ultraviolet light for state-of-the-art nanolithography. Currently, CO_2 lasers are used to drive the plasma. In the future, solid-state mid-infrared lasers may instead be used to efficiently pump the plasma. Such laser systems have promise to be more compact, better scalable, and have higher wall-plug efficiency. In this Topical Review, we present recent findings made at the Advanced Research Center for Nanolithography (ARCNL) on using 1- and 2-μm-wavelength solid-state lasers for tin target preparation and for driving hot and dense plasma. The ARCNL research ranges from advanced laser development, studies of fluid dynamic response of droplets to impact, radiation-hydrodynamics calculations of, e.g., ion "debris", (EUV) spectroscopic studies of tin laser-produced-plasma as well as high-conversion efficiency operation of 2-μm-wavelength driven plasma.

I. INTRODUCTION

Multiply excited states in multiply charged tin ions, bred in laser-produced transient plasma, are responsible for emitting narrow-band extreme ultraviolet (EUV) light at 13.5-nm wavelength [1] for nanolithography. EUV lithography (EUVL) has successfully entered high-volume manufacturing. EUVL enables the continued shrinking of electronic devices as captured by Moore's law. This law drives the semiconductor industry [2, 3] by postulating, or rather by demanding, that the number of transistors on an affordable CPU doubles every two years [4, 5]. The production of any semiconductor device is a repetitive opto-chemical process. Photolithography is a key step in this device manufacturing [6, 7]. It is a photochemical process in which a thin layer of material, a photoresist, is exposed to light. This light images onto the photoresist a so-called mask that is imprinted with the desired shapes, or "features". Photolithography is the defining step in setting the minimum obtainable feature size on a device. Following Abbe's law of limiting resolution, the shorter the wavelength of the light used, the better the resolution. The better the resolution, the smaller the features that can be produced. EUVL, at 13.5-nm wavelength, can thus be seen as the logical, if ambitious, next step from using 193-nm light that is still used for many lithography applications. The production of the required EUV light at sufficient power, within a narrow "in-band" 2% wavelength bandwidth centered at 13.5 nm that can be reflected by multilayer optics [8, 9], continues to present both industry and science with physics challenges, in particular in the optics and photonics fields.

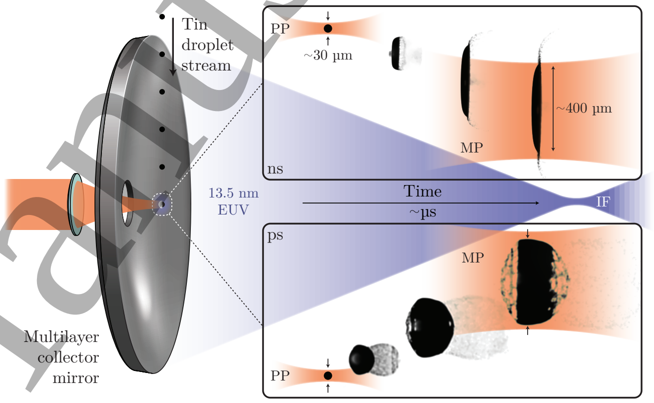

FIG. 1. Schematic illustration of droplet-based EUV source operation using a pre-pulse (PP) plus main-pulse (MP) irradiation scheme including actual shadowgraph images. The top panel shows the typical deformation occurring after impact of a ns-duration pre-pulse and the lower panel the expansion following impact of a ps-duration pre-pulse. In both cases a typical desired target size is attained after several μs, at which point the target is irradiated by a more energetic main pulse, generating plasma that emits 13.5 nm EUV radiation. The EUV light is collected by the multilayer "collector" mirror and focused at the intermediate focus (IF), the entry point of the illuminator part of an industrial wafer stepper machine. Illustration and caption are reproduced and modified, respectively, from Ref. [10] with permission from the author.

Following our 2019 review [11], there are several crucial requirements for EUV light sources. Such sources should have high conversion efficiency (CE). Here, CE is defined as the ratio of in-band EUV light emitted into a half-sphere backwards towards the laser (this half-sphere being covered by the collector mirror, see Fig. 1) over the laser energy used to obtain it. From the per-

---

[*] o.versolato@arcnl.nl

spective of sustainability, the total efficiency of converting wall-plug electricity to useful EUV light is another relevant performance indicator. Next, the amount of optics-lifetime-limiting-debris that the plasma produces (typically consisting of fragments or high-energy particles) should remain manageable. Historically, there were three promising candidate elements: Li, Sn and Xe, all of which have ions with strong electronic resonance transitions within the required bandwidth. However, for various reasons, the reported CE of Li- and Xe-based plasma sources are much lower than that of Sn-based plasmas [12, 13]. Current state-of-the-art sources of EUV light are based on the irradiation of so-called mass-limited, micrometer-sized droplets of molten tin by high-energy CO_2-laser pulses of 10.6-μm wavelength at several 10-kHz repetition rates, which creates an EUV-emitting laser-produced plasma (LPP) in several steps cf. Fig. 1.

First, a low-energy pre-pulse deforms a spherical tin droplet into a target shape optimized for interacting with a high-energy main pulse. This deformation process involves a plethora of physical processes, ranging from laser-matter interaction, to plasma radiation-hydrodynamics, to pure fluid mechanics - with a clear separation of the relevant time scales. The ordering of these time scales determines to a large degree the overall target morphology [10, 14]. On one extreme end, short fs-ps laser pulses create bubble-like targets (see Fig. 1 bottom panel) as described by, e.g., Kurilovich *et al.* [15] (also see Refs. [16–20]) and more recently by De Faria Pinto *et al.* [21] addressing also laser polarization dependencies. On the other extreme end, long (ns) laser pulses create strongly propelled, flattened targets (see Fig. 1 upper panel). The industry has opted for using relatively long (∼10 ns) laser pulses, creating a quasi-stationary, strongly radiating plasma ablation front that leads to the propulsion [22–24] and the required deformation of the droplet [22, 23, 25, 26] into a "pizza" target shape (see Section II), i.e. a relatively flat thin disk bounded by a thick rim [27, 28]. Subsequent pulses of even lower energy may be used to rarefy a tin target in order to, e.g., make a preheated plasma [29] that is later to be laser-reheated [13, 30, 31]. Vaporization of the several 10 nm thick targets [27] can also be employed to obtain further information about the thickness profile itself.

Next, a high-energy laser main pulse drives the dense plasma from the target as prepared by the preceding pre-pulse(s). In industrial sources of EUV light the drive laser light is obtained from high-power CO_2-gas lasers operating at a wavelength of 10.6-μm [32]. Solid-state laser systems, typically operating at a shorter near-infrared wavelength could potentially provide an attractive alternative [33, 34] to the gas laser technology for driving the plasma (see Section III) with the promise of higher wall-plug efficiency and reduced complexity. Understanding the origins of the plasma-emitted EUV light, and thus the complex atomic structures of multiply charged tin ions (Section III A) is crucial to be able to optimize future sources through predictive modeling [35]. Given the size of the outstanding challenges and the impact of new developments on society, it should not come as a surprise that modeling efforts have been stepped up worldwide. The Code Comparison session in the yearly EUV Source Workshop, organized jointly by EUV Litho, Inc. [36] and ARCNL since 2019, has the ambition to bring together plasma modelers to improve simulation capabilities of EUV sources [35]. Besides the in-band EUV, there is interest in out-of-band (OOB) radiation in the EUV and also in the deep-ultraviolet (DUV) range. This OOB radiation may be detrimental for imaging contrast [37, 38], but can also provide a unique window into the radiative heart of the plasma motivating detailed spectroscopy efforts [39–41]. Predictive modeling should also take the expansion of the hot and dense plasma into account: ions may reach typical kinetic energies of several keV (Section III B). The impingement of such energetic particles on nearby optical elements may be detrimental for their performance. As such, plasma expansion and the generation (and stopping) of energetic particles is a subject of particular interest [42–47]. Producing the currently required 250 W of EUV light at the so-called intermediate focus (IF), where the source is connected to the scanner, has been a daunting, and continuing challenge. The semiconductor roadmap now asks for a stable 1000 Watt (at IF) source, quadrupling the present source performance. This calls for game-changing innovation driven by research at the fundamental level.

This topical review builds on a review from 2019 on the topic by Versolato *et al.* [11], itself building on the earlier work of Banine *et al.* [43] of ASML and indeed on the work of many others, e.g., of the University College Dublin (UCD) Spectroscopy Group, Lawrence Livermore National Lab (LLNL), Los Alamos National Laboratory (LANL), the Center for Materials Under eXtreme Environments (CMUXE) at Purdue University, the Institute of Spectroscopy of the Russian Academy of Sciences (ISAN), the Keldysh Institute of Applied Mathematics (KIAM), the Laboratory for Energy Conversion at ETH Zürich, the EUV Photonics Laboratory of the University of Central Florida, the Institute of Laser Engineering of Osaka University, Tokyo Metropolitan University and Gigaphoton (and still many others). This review will combine an overview of recent, relevant literature with discussions of key processes that govern the dynamics in each step in the process of generating EUV light, while focusing on recent results from the Source Department of the Advanced Research Center for Nanolithography (ARCNL) in Amsterdam. ARCNL is tasked to focus on the fundamental physics and chemistry behind current and future technology for nanolithography, especially for application in the semiconductor industry.

II. LASER-DROPLET INTERACTION FOR TIN TARGET PREPARATION

Current high-power industrial EUV sources are based on the pulsed irradiation of a high-frequency stream of micrometer-sized droplets of molten tin. The reason for using individual, well-separated droplets is that each droplet serves as an isolated reservoir of tin with limited mass. Such mass-limited targets enable careful optimization of CE while using a minimum amount of tin and, moreover, generate a minimal amount of debris. The careful shaping of a spherical droplet into a shape optimally suited for interaction with the energetic main pulse is key for such careful optimization and control.

The transformation of a spherical tin droplet into a suitable target using laser "pre-pulses" involves a broad range of physical processes. Of key importance for the final morphology of the target is the ordering of the time scales associated with the various physical processes. Among the shortest timescales is the electron-ion relaxation time $\tau_{e-i} \sim 10\,\text{ps}$, which is related to the exchange of energy between electron and ion subsystems, with the electron subsystem directly heated by the laser pulse through the process of inverse brehmsstrahlung.

The next longest time scale is the plasma-hydrodynamic time scale, which is set by the ratio of the plasma flow length scale distance to the velocity of this flow. This flow length scale, i.e., the distance between droplet and critical surface (where the plasma electron density exceeds the critical density for the incoming laser beam) is of order $\sim 10\,\mu\text{m}$ and the typical flow velocity is given by the speed of sound in the laser produced plasma corona $\sim 10^5\,\text{m/s}$ [48]. Together they yield a hydrodynamic time scale $\tau_h \sim 100\,\text{ps}$ [48]. Next is the acoustic time scale of the tin liquid τ_a on which pressure waves, launched by the plasma produced by the laser pulse, acoustically travel (with sound speed $c \sim 2500\,\text{m/s}$) through the droplet (with radius $R_0 \sim 25\,\mu\text{m}$), $\tau_a \sim R_0/c \sim 10\,\text{ns}$. This time scale is followed by the inertial time scale $\tau_i = R_0/U \sim 100 - 1000\,\text{ns}$ on which the droplet relevantly deforms. Following the practice well-established in the fluid dynamics literature, the typical deformation velocity is here taken to be the propulsion, or impact velocity $U \sim 100\,\text{m/s}$. This impact velocity should be compared to the more relevant velocity $\dot{R}_0$, the initial radial expansion rate. Typically $\dot{R}_0 \sim U$, however the precise relation depends on, e.g., how tightly the laser is focused onto the droplet. More tightly focused beams lead to larger $\dot{R}_0$ (and $\dot{R}_0 > U$). Hernandez-Rueda *et al.* [49] have explored a large parameter space to investigate the influence of the tin droplet diameter as well as the laser beam diameter and energy on the $\dot{R}_0/U$ ratio. Next, they compared the experimental U and $\dot{R}_0$ values to those obtained with detailed radiation-hydrodynamic simulations using the RALEF-2D code which in turn enabled validating analytical fluid-dynamics modeling [26].

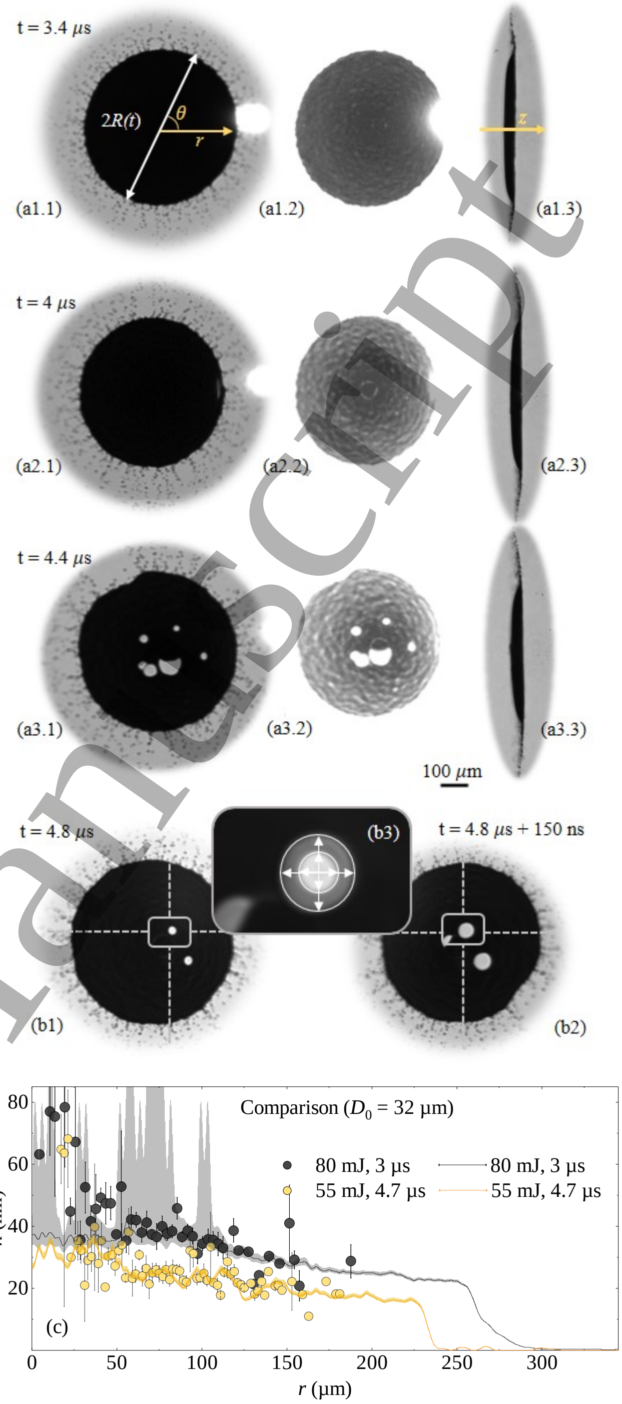

FIG. 2. Shadowgraph images of expanding sheets from tin microdroplets hit by a ns laser pulse. (a1.1, a2.1, a3.1) Front views of liquid sheets at time delay t (laser impacts at $t = 0$). The bright spot visible in several of the images is from plasma emission. (a1.2, a2.2, a3.2) Same images with a digitally modified contrast. (a1.3, a2.3, a3.3) Corresponding side-view images (laser impacts from the left, propelling the droplet to the right). In (a1.1, a1.3), the cylindrical coordinate system (r, θ, z) with its origin at the center of sheet is depicted. At later times, holes appear cf. (a3, b1, b2). The overlay of a hole is highlighted by a white box in both (b1, b2). The arrows in inset (b3) indicate the receding edge of the hole the velocity of which gives the local thickness (see main text). (c) Sheet thickness as a function of the radial coordinate. Comparison of results obtained using a backlight-transmission method (cf. panel [a2.2]) and from a complementary method using hole-opening velocities (cf. panel [b1,b2]). Figure and caption modified from Ref. [28].

The near-equivalence $\dot{R}_0 \sim U$ may break down if the laser pulse is of particularly short duration ($\dot{R}_0 \gg U$ with $U \approx 0$, cf. Fig. 1).

Last in line is the capillary time scale $\tau_c = \sqrt{\rho R_0^3/\sigma} \sim 10\,\mu$s, with liquid density ρ and surface tension σ [26]. This is the time scale on which retraction of the sheet due to surface tension occurs. Theoretical work by Reijers *et al.* [14], recently experimentally validated by Meijer *et al.* [10], made clear that the time scale of significant changes in laser intensity (typically of the order of the laser pulse duration τ_p) over the time scale ordering $\tau_{e-i} < \tau_h < \tau_a < \tau_i < \tau_c$ is a crucial factor determining the fluid-dynamic deformation of the droplet and final target morphology.

From the whole palette of pre-pulse settings, the EUVL industry has opted for using relatively long ($\tau_p \sim 10$ ns) laser pulses which, given that $\tau_p \gg \tau_h$ [48], create a quasi-stationary plasma that leads to the propulsion and the required deformation of the droplet into a relatively flat, thin disk bounded by a thick rim. This "pizza" shape was uncovered and experimentally mapped in detail by Liu *et al.* [28], who studied the morphology of a radially expanding sheet of liquid tin formed by ns-pulse Nd:YAG laser impact on a spherical microdroplet. Specifically, the sheet thickness profile and its time evolution were captured over a range of laser-pulse energies for two droplet sizes. Two complementary methods were employed to determine the thickness profile. In the first method, the finite transmissivity of the several 10-nm thick stretched liquid-metal sheet was recorded and, with the known optical constants of tin [50], the transmissivity could be converted to a local thickness $h(r)$ as a function of the radial coordinate r (see Fig. 2[a1.2,a2.2]). In the second method, the speed of opening of spontaneously formed holes (cf. Fig. 2[b1–3]) in the stretching sheet is experimentally measured, which again allows one to obtain $h(r)$ following Culick [51]. Results from the two methods, indicating the presence of a thin tin sheet just several 10 nm in thickness, were shown to be in excellent agreement cf. Fig. 2(c). Moreover, all obtained thickness profiles were shown to collapse onto a single self-similar curve enabling the prediction of the thickness profile under a wide range of experimental conditions.

Spatial integration of the thickness profiles enables one to determine the volume of the sheet as a function of time after pre-pulse laser impact, see Fig. 3. Remarkably, less than half of the initial amount of tin remains in the sheet under these conditions. Further analysis shows that the largest fraction of the mass lost from the sheet during its expansion ends up as fine fragments (see Fig. 3). Liu *et al.* [28] proposed that such mass loss can be minimized by producing the sheet targets on the shortest possible timescales. A follow-up study validated this proposal, where Liu *et al.* [27] irradiated thin tin sheets with a low-intensity laser pulse. This auxiliary pulse, used as a probe with an intensity below plasma threshold (following Meijer *et al.* [52]), induced vaporization which enabled investigation of the thickness profile of the sheet and its mass also at earlier times (see Fig. 3). The results demonstrated that increasing the energy of the Nd:YAG laser pulse, which enabled reaching the predetermined target radius more quickly, resulted in a larger mass fraction remaining in the sheet. As a corollary, less tin ended up in other channels of the mass distribution such as fragments surrounding the sheet, thus leaving more mass in the target sheet available for interaction with the more energetic main laser pulse to produce EUV light.

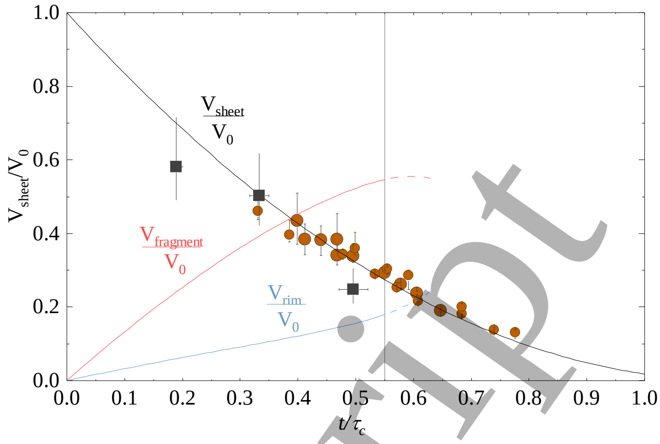

FIG. 3. Volume ratio of the sheet to that of the initial droplet V_{sheet}/V_0 as a function of non-dimensional time t/τ_c for various droplet sizes and Weber numbers (see Ref. [28]). Brown data (circles) are obtained from Ref. [28] using the method illustrated in Fig. 2. Dark gray data (squares) are obtained from a laser vaporization method [27]. The analytical prediction for V_{sheet}/V_0 is presented as a black solid line. The inferred volume ratios V_{rim}/V_0 and V_{fragment}/V_0 are presented as blue and red lines, respectively, following Ref. [28]. The vertical line marks $t/\tau_c \approx 0.55$ from where the model validity is unclear. Figure data taken from Refs. [27, 28].

III. MAIN PULSE: USING SOLID-STATE LASERS TO DRIVE EUV EMISSION

Once a suitable target shape is reached, the main laser pulse transforms the liquid target into a hot and dense EUV emitting plasma [11, 73]. In the industry, the laser providing these pulses currently is an infrared 10.6-µm wavelength CO_2 gas laser. Tin plasma driven at this laser wavelength has particularly high CE (see Fig. 4). Solid-state lasers, typically operating at shorter, near-infrared wavelengths may soon be able to provide a viable alternative to these CO_2 gas lasers [74]. Such solid-state laser systems may be more compact and have higher wall-plug efficiencies. Reducing the drive laser wavelength from 10.6-µm will, however, also increase the typical tin ion densities in the region where EUV light is generated in the plasma. This effect can be qualitatively understood [11] from the increase in critical electron density n_c with decreasing drive laser wavelength λ through $n_c \sim \lambda^{-2}$.

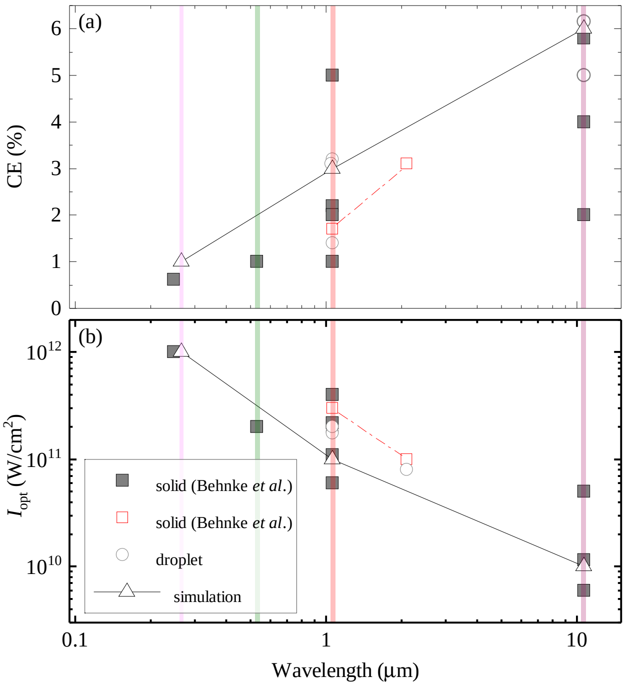

FIG. 4. (a) Conversion efficiency (CE) and (b) optimum laser intensity (I_{opt}) values as a function of drive laser wavelength as obtained from previous experiments on planar solid (full gray squares) and droplet (open gray circles) tin targets (data from Refs. [53–72]). Overlapping data points are shifted vertically for visibility. Simulation results [12] for plasma under optimal conditions are shown (open black triangles) connected by straight lines. The vertical lines, moving from right to left, indicate the wavelengths of CO_2 laser light, Nd:YAG laser light (fundamental), as well as the second and fourth harmonics of Nd:YAG laser light. The results of the work of Behnke *et al.* [34] are shown as open red squares (see main text). Reprinted with permission from Ref. [34] © The Optical Society.

Beyond n_c, where the electron plasma frequency is equal to the laser light frequency, laser light cannot propagate. Relevant plasma densities increase at a slower pace $\sim \lambda^{-1}$ [72] (see below), but nevertheless the plasma gets more dense with decreasing drive laser wavelength. Increased plasma density is associated with larger optical depths (the product of atomic opacity, mass density, and path length [72, 75]), which causes opacity broadening of the 13.5 nm emission feature beyond the 2% acceptance bandwidth, thus reducing the spectral purity (SP, defined as the ratio of spectral energy in a 2% bandwidth around 13.5 nm to the total EUV energy) and with it the maximally obtainable CE [55, 61, 63, 65, 71, 75–77].

Nishihara *et al.* [12] provided simulation results for optimal drive laser intensities, with predictions for obtainable CE for idealized "0-D" plasmas. In Fig. 4(a), CE values from the simulations are indeed shown to increase with increasing drive laser wavelength. The optimum laser intensity decreases with increasing laser wavelength (and, thus, with decreasing plasma density). Several recent simulation efforts (see, e.g., Ref. [33]) have drawn the attention of the EUV source community to the use of a 2 μm drive laser, further supported by the recent introduction of novel concepts for high-power solid-state laser systems operating at this wavelength. Such promising simulations are particularly challenging, not least because of the complex atomic physics involved, and require experimental benchmarks.

Schupp *et al.* [72, 78], and Behnke *et al.* [34] recently reported the first experimental study of 2 μm laser-driven tin plasmas. These studies, discussed in Section III C, confirmed the simulation results with regards to the particular promise of the 2 μm driver. Additional experiments are required in unison with detailed predictive modeling efforts. The modeling efforts need as input accurate atomic physics data to enable understanding the origins of the plasma-emitted EUV light. These origins, discussed in Section III A, were recently shown to be much more complex than previously thought. Predictive modeling should also take into account the expansion of the hot and dense laser-driven plasma, where ions reach kinetic energies on the order of several keV. This topic will be discussed further in Section III B. The development of advanced solid-state laser systems at ARCNL will enable dedicated studies to find the true optimum conditions to drive tomorrow's plasma sources of EUV light, as we conclude in Section IV.

A. Strong contributions of multiply excited states to EUV emission

The complex electronic structures of multiply charged tin (Sn) ions are the root cause of their particular attractiveness for use in next-generation nanolithography [3, 11, 32, 43, 70, 79, 80]. They are employed as emitters of in-band 13.5 nm EUV photons. The suitability of Sn ions for this application stems from their open-$4d$-subshell structures [39, 81–90]. Within these structures, $\Delta n = 0$ one-electron-excited configurations are well-known to decay to the ground state manifold via a multitude of transitions clustered together in unresolved transition arrays (UTAs) [91] centered around 13.5 nm. An exceptional feature of Sn ions is the fact that the average excitation energies of these configurations are similar across the isonuclear sequence Sn^{11+}–Sn^{14+}, making these charge states excellent radiators of 13.5-nm light. Recently, however, a team of researchers from ARCNL and Los Alamos National Laboratory (LANL) found that the characteristics of Sn ions are even more special and that the EUV light generated in these plasmas originates predominantly from transitions from multiply excited states [1]. Contrary to the prevailing view, contributions from one-electron-excited states are not the prime sources of EUV light in the in-band spectral region. This serendipitous alignment of transitions in singly, doubly, and triply excited systems occurs over a range of charge

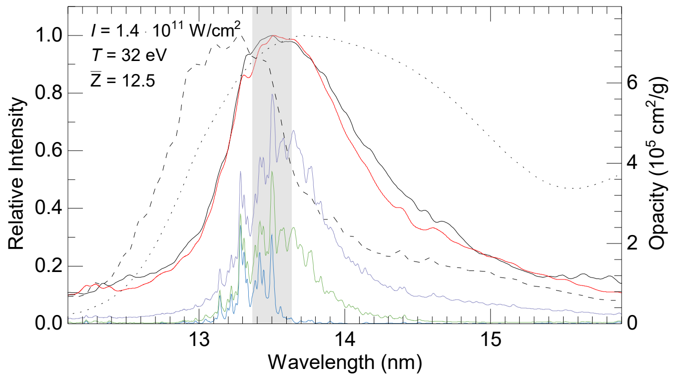

FIG. 5. Comparison of atomic opacity calculations with an experimental spectrum using a 1D radiation transport through a single-density (0.002 g cm^{-3}), single-temperature plasma (32 eV) - see main text. Experimental spectrum (black solid line) and calculated flux (red solid line) are shown, normalized to their respective maxima. The dashed and dotted lines show the spectral fluxes calculated from the opacity spectrum reported in Ref. [89] and HULLAC calculations [76], respectively. The individual contributions to the opacity spectra are also shown. The mean charge state of the calculated plasma is $\bar{Z} = 12.5$. The grey area highlights the industrially-relevant 2 % bandwidth centered at 13.5 nm. Figure and caption modified from Ref. [1].

states Sn^{11+}–Sn^{14+}. The work [1] revealed the doubly magic behavior of tin and the origins of the EUV light.

The importance of the multiply excited states for the EUV emission is demonstrated in Fig. 5, where a comparison between an experimental emission spectrum (black curve, produced from plasma generated by impinging a Nd:YAG laser pulse onto a tin microdroplet) and the spectral flux obtained from one-dimensional radiation-transport modeling (red curve, which uses as input the ATOMIC opacity calculations) is shown [1]. The spectral flux calculated using a single-density, single-temperature approach clearly reproduces the measured emission strikingly well. Without the contributions from the multiply excited states, it would clearly not be possible to explain the experimental spectrum to any degree of satisfaction. To further highlight the importance of these transitions, as well as the accuracy of the work of Torretti *et al.* [1], the results are compared with calculations from previous works [76, 89].

In follow-up work by Sheil *et al.* [92], the Los Alamos ATOMIC code was used to investigate the spectral contribution from transitions from multiply excited states in CO_2 laser-driven ($\lambda = 10.6$ µm) tin plasma conditions. Here, in comparison the Nd:YAG drive laser case, much lower plasma densities are obtained where local-thermodynamic equilibrium (LTE) conditions are not met. Busquet's [93] ionisation temperature method was employed to match the average charge state of a non-local-thermodynamic equilibrium (non-LTE) plasma with an LTE one, establishing a so-called ionization temperature T_Z. This approach is found to generate LTE-computed configuration populations in excellent agreement with the non-LTE populations. A corollary of this observation is that the non-LTE populations are well-described by Boltzmann-like exponential distributions characterized by the effective temperature T_Z. Subsequently, extensive level-resolved LTE opacity calculations were performed at T_Z. Sheil *et al.* [92] also found that the leading contributions to the opacity near 13.5 nm arise from transitions from multiply excited states. These results reinforce the need to include multiply excited states in atomic models from which the radiative properties of laser-driven tin plasmas are generated. The work of Sheil *et al.* [92] paves the way for the generation of detailed LTE opacity tables at non-LTE plasma conditions, which can be incorporated in radiation-hydrodynamic simulations of laser-driven tin plasmas. Such simulations will enable reliable predictions of EUV emission from LPPs and will play a key role in guiding experimental efforts in the characterization and optimization of laser-driven plasma sources of EUV light.

Aside from the in-band EUV radiation, spectroscopy in other wavelength ranges can provide further valuable insight into the properties of the laser-driven tin plasma. Indeed, detailed information about the contribution of the various charge states to the main 13.5 nm emission feature can be obtained from out-of-band transitions. Short-wavelength emission, located between 7 and 12 nm, enables the assessment of the charge state distribution [39, 40] and served to diagnose industrial CO_2-laser-driven plasmas as demonstrated by Torretti *et al.* [41]. Using the method developed by Scheers *et al.* [94] for charge-state-resolved spectroscopy, Bouza *et al.* [95] compared laser-driven plasma emission with electron beam ion trap spectroscopies at longer EUV wavelengths. This plasma spectroscopy work was later extended to include deep ultraviolet (DUV) and UV wavelengths, where an intensity-calibrated spectrum from 5 all the way up to 265 nm wavelength [96] was recorded using a novel transmission grating spectrometer (TGS) developed by the MESA+ XUV Optics group at Twente University, in tandem with a smart choice of filters. The TGS will soon be upgraded with one-dimensional imaging capabilities, enabling space-resolved characterization of plasma ionicity (see Byers *et al.* [97]). Scheers *et al.* investigated the UV and optical emission from the lower charge states in the plasma [98]. This work was followed by a temporally and spatially resolved study of the optical emission from these lower charge states, where the evolution of electron density and temperature in the "afterglow" of the LPP was quantified using a fiber-coupled imaging spectrometer [99]. Further spectroscopic studies will undoubtedly drive predictive modeling efforts and the development of future EUV light sources.

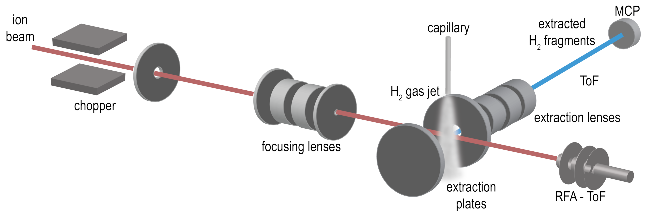

FIG. 6. Schematic view of the crossed-beam setup that will be used to measure charge exchange and energy loss in the forward-scattering direction by means of a combined electrostatic Time-of-Flight analyzer system, while target fragments from the interactions of Sn^{q+} ions colliding with H_2 are extracted sideways into a Time-of-Flight spectrometer. The full setup can be operated on high voltage to decelerate the incoming ion beams allowing for a coverage of the full kinetic energy range of plasma ions from close to 0 to tens of keV.

B. Plasma expansion - "fast ionic" debris

Besides the sought-after EUV light, a laser-produced plasma produces debris in the form of fast ions, the impact of which may limit the lifetime of the light collecting multilayer optics. Rai *et al.* [100] studied single-collision scattering of keV-energy ions off surfaces to elucidate the absence of a single-scattering peak in the here relevant Sn-Ru collisions [101] and to test the predictive power of standard Monte Carlo binary collision codes such as SRIM (Stopping and Range of Ions in Matter) [102]. These codes, which were primarily developed for modeling swift particle interactions with solid state targets, are also used to simulate the stopping and mitigation of plasma ions in hydrogen buffer gas surrounding the plasma. Corresponding experimental data on slow ($E \leq$ 100 eV/amu) heavy ions is by and large lacking. To investigate the interactions between Sn^{q+} ions with H_2 we have commissioned an advanced crossed-beam type setup based on experience from previous crossed-beam experiments [103, 104], see Fig. 6.

Fast plasma ions are generated during the expansion phase of the plasma [105]. Understanding such plasma expansion at the fundamental level is key for modeling the laser-produced plasma. Hemminga *et al.* [106] presented the results of a joint experimental and theoretical study of plasma expansion driven by Nd:YAG laser ablation (laser wavelength $\lambda = 1.064\ \mu m$) of tin microdroplets under conditions relevant for nanolithography. The experimental measurements indicate a near-plateau in the ion energy distribution for kinetic energies in the $0.03 -$ 1 keV range, a peak near 2 keV followed by a sharp fall-off in the distribution for energies above 2 keV (red curve in Fig. 7). Charge-state resolved measurements, performed with a cross-calibrated electrostatic analyzer in time-of-flight mode (ESA-ToF) [107], attributed this peaked feature at 2 keV to the existence of peaks (centered near 2 keV) in the $\text{Sn}^{3+} - \text{Sn}^{8+}$ ion energy distributions. To understand the physical origin of this peaked feature, Hemminga *et al.* [106] performed two-dimensional simulations of the plasma initiation, growth and subsequent expansion using the radiation hydrodynamic code RALEF-2D. As is evident from Fig. 7, excellent agreement was found between the simulated ion energy distribution and the measurements both in terms of the shape of the distribution and the absolute number of detected ions. The peak in the ion energy distribution near 2 keV was attributed to a quasi-spherical expanding shell formed at early times in the expansion.

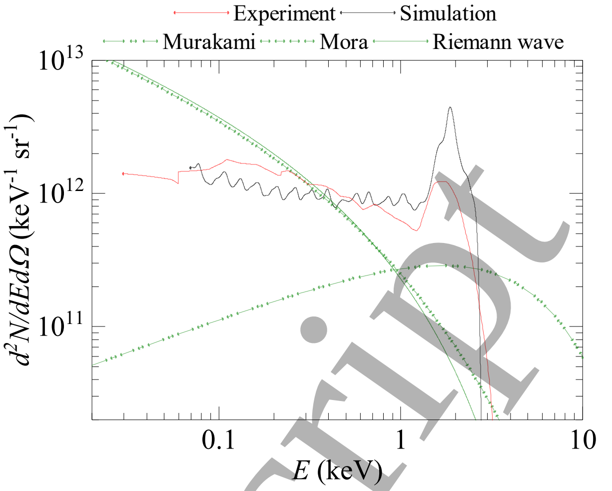

FIG. 7. The distribution of the number of ions over ion kinetic energy. The experimental ion energy distribution is shown in red (solid curve) and the RALEF-2D ion energy distribution is shown in black (solid curve). Also illustrated in green are the predictions of analytic models of plasma expansion (see discussion in Ref. [106]). Figure and caption reproduced from Ref. [106].

These results demonstrate that the single-fluid single-temperature approach implemented in RALEF-2D can not only reproduce the general shape of the experimental ion energy distribution, but it can also provide a reliable prediction for the absolute number of ions, thus paving the way for future predictive modeling of plasma EUV light sources.

C. Comparing plasmas driven by 1- and 2-μm-wavelength lasers

Recent simulation efforts at Lawrence Livermore National Laboratory (LLNL, and see, e.g., Ref. [33]) have indicated that use of a drive laser at ∼2 µm wavelength may be particularly beneficial for driving the tin plasma. Concurrently, LLNL introduced the concept of high-energy, high-power Big Aperture Thulium (BAT) laser systems operating at 1.9 µm wavelength.

At ARCNL, experiments were started to investigate the potential of such novel lasers and novel wavelengths to drive plasma. Behnke *et al.* [34] were the first to present an experimental study of a 2-µm laser-driven tin

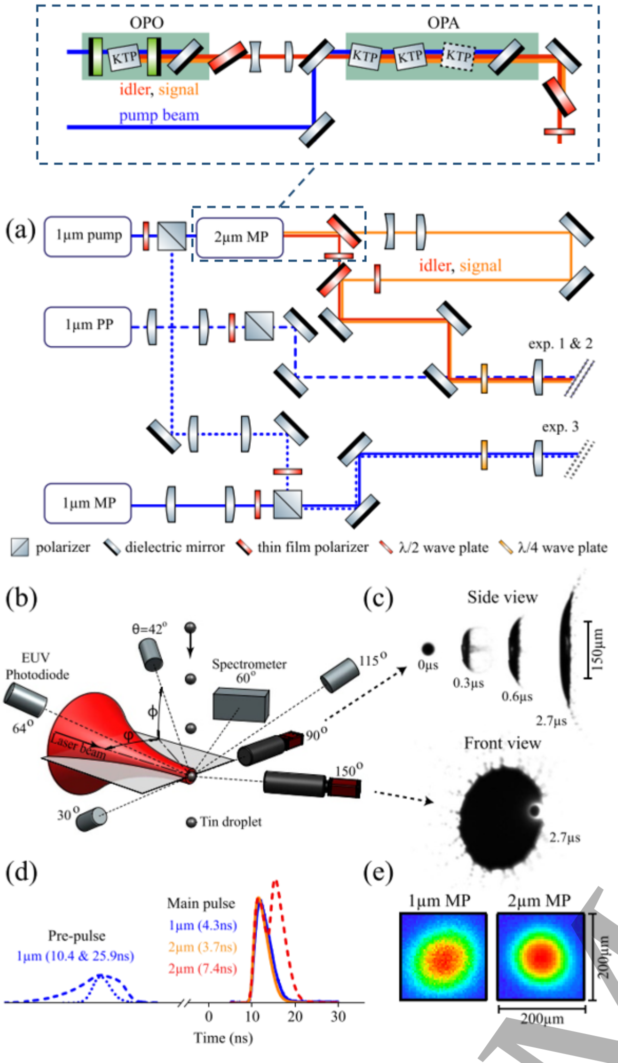

FIG. 8. (a) Schematic representation of the laser beam setups adopted in the experiments described in Schupp *et al.* [78] using a pre-pulse (PP) to predeform droplet targets before impact of the main pulse (MP) lasers. The top inset, taken from Ref. [72], shows a master oscillator power amplifier (MOPA) setup (see main text). (b) Continuation from (a) showing the locations and angles of the various detectors. (c) Selection of front- and side-view shadowgraphs of the tin targets used for plasma generation, recorded by the two cameras indicated in (b). (d) Temporal and (e) spatial profiles of the laser beams. Figure and caption modified from Ref. [72, 78].

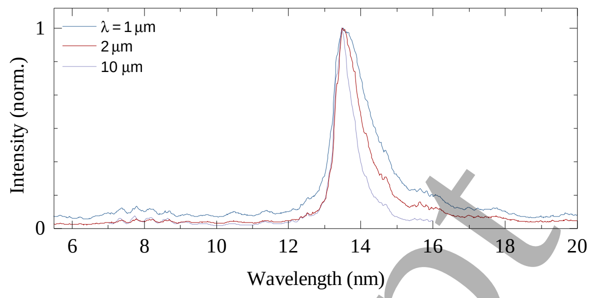

FIG. 9. EUV spectrum produced with a 2-μm laser-driven tin plasma (red line) compared to that obtained from a 1-μm laser-driven plasma (blue line). Also shown is a spectrum obtained using a 10-μm CO_2 laser that here represents the case of small optical depth (reproduced from Ref. [108] in Ref. [72]). Figure and caption modified from Ref. [72].

plasma in which a planar tin target was irradiated with laser pulses of 5 ns duration. The 2-μm laser light source (cf. Fig. 8(a) inset) used comprised a potassium titanyl phosphate (KTP) based master oscillator power amplifier (MOPA) operated in type-2 phase matching. The MOPA is pumped at a 10 Hz repetition rate by a seeded, Q-switched Nd:YAG laser providing pulses of 10 ns duration. First, a 2170 nm idler seed beam is created in a singly-resonant optical parametric oscillator (OPO). To create the seed beam, a fraction of the pump light is demagnified to a beam diameter of 1.5 mm and is coupled into the OPO, operated in a collinear alignment. About 20% of the pump radiation is converted into a 2090 nm wavelength signal beam and a 2170 nm idler beam. A dichroic mirror separates the signal and idler beams from the partially depleted pump. The idler beam is subsequently expanded to 11 mm in diameter to seed the optical parametric amplifier (OPA), while the signal beam is removed through polarization optics. The OPO and OPA are pumped by the same laser. For pumping the OPA, 1.3 J of the Nd:YAG laser light is delayed by 1.3 ns and is reduced to a beam size of 10 mm in diameter. Seed and pump beams are overlapped on a dichroic mirror after which they pass several 18-mm-long KTP crystals. The crystal orientation is alternated to compensate for walk-off. A total (sum + idler) energy of several 100 mJ can routinely be achieved. Pump and signal beams are separated from the idler using a dichroic mirror and polarization optics, respectively. To adjust the energy of the idler beam, a waveplate/polarizer combination is employed before focusing the beam onto the target. The size of the focal spot was approximately $100 \times 100\,\mu m^2$. Spectroscopic investigations were performed for plasmas driven by this 2-μm-wavelength pulsed laser light and comparisons were made with plasmas driven by the 1-μm pump laser light at several laser intensities. Very similar EUV spectra, and thus underlying plasma ionicities, were obtained when the intensity ratio was kept fixed at I_{1m}/I_{2m} = 2.4(7). Crucially, the CE was found to be a factor of two larger (at the given 60 degree observation angle) for the 2-μm-laser-driven plasma compared to the case of the denser, 1-μm-driven plasma.

Following soon after, Schupp *et al.* [72] presented experimental spectroscopic studies of EUV light emitted from plasma produced by the irradiation of tin microdroplets with 5-ns-pulsed, 2-μm-wavelength laser light (cf. Fig. 8) using the same laser system as in Ref. [34]. Emission spectra were compared to those obtained from plasma driven by 1-μm-wavelength Nd:YAG laser light over a range of laser intensities. Over the studied range of drive laser intensities, it was found that similar spectra (and thus underlying plasma charge state distributions) were obtained when the ratio of the 1-µm to 2-µm laser intensities was fixed at a constant value, in good agreement with the findings of Behnke *et al.* [34]. Schupp *et al.* [72] also performed laser-plasma simulations using the radiation-hydrodynamic code RALEF-2D and found good agreement regarding the intensity ratio. Their experimental findings, supported by the simulations, indicate an approximately inversely proportional scaling $\sim \lambda^{-1}$ of the relevant plasma electron density and the aforementioned required drive laser intensities with drive laser wavelength λ in line with the predictions of Nishihara *et al.* [12] (cf. Fig. 4) for a plasma system of much reduced complexity. The $\sim \lambda^{-1}$ scaling was also found to extend to the optical depth as captured in the observed changes in spectra over a range of droplet diameters. The decrease of optical depth with increasing drive laser wavelength is illustrated in Fig. 9, where experimental spectra from 1, 2, and 10-µm drivers are seen to decrease in width with increasing λ.

In a detailed follow-up work, Schupp *et al.* [78] reported on the EUV emission properties of tin plasmas produced by the irradiation of pre-pulse-preformed liquid tin targets by 2-µm-wavelength laser pulses (cf. Fig. 8). In a two-pulse scheme, much like in the current industrial setting, a pre-pulse laser is first used to deform tin microdroplets into thin, extended disks (cf. Fig. 8(c)) before the main (2 µm) pulse creates the EUV-emitting plasma. The effects of a change in 2-µm drive laser intensity and laser pulse duration (3.7–7.4 ns; for the longer pulses, both signal and idler were used) were studied. It was found that the angular dependence of the emission of light within a 2% bandwidth around 13.5 nm and within the backward 2π hemisphere around the incoming laser beam is almost independent of intensity and duration of the 2-µm drive laser. With increasing target diameter, the emission in this 2% bandwidth becomes increasingly anisotropic, with a greater fraction of light being emitted into the backward 2π hemisphere around the incoming laser beam. For direct comparison, a similar set of experiments was performed with a 1-µm-wavelength drive laser. EUV emission spectra were found to exhibit prominent self-absorption of light around 13.5 nm in the 1-µm case, while in the 2-µm case only a modest opacity-related broadening of the spectral feature at 13.5 nm was observed. The work demonstrated the enhanced capabilities and performance of 2-µm-driven plasmas produced from disk targets when compared to 1-µm-driven plasmas both in terms of CE (cf. Fig. 10(a)) and SP (cf. Fig. 10(b)).

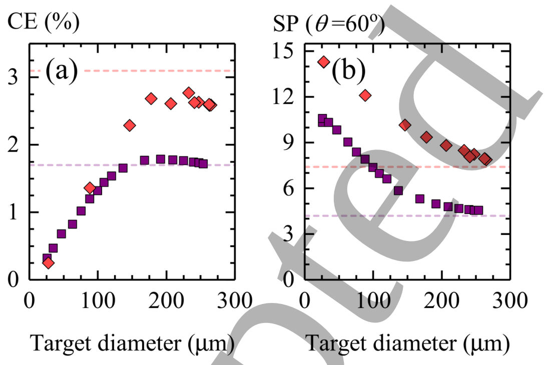

FIG. 10. Comparison of results for drive laser beams of 1- (solid purple squares) and 2-µm (solid orange diamonds) wavelength at intensities of 1.9 and 1.0×10^{11} W/cm^2, respectively. (a) CE and (b) SP as a function of target diameter. The dashed lines in (a) and (b) indicate the CE and SP values obtained from laser-irradiated, planar-solid tin targets, respectively [34]. All SP values provided are calculated with respect to the measured spectral range of 5.5–25.5nm. Figure and caption modified from Ref. [78].

The significant improvement of the spectral performance of the 2-µm- vs 1-µm-driven plasma provides strong motivation for the development of high-power, high-energy near-infrared lasers to enable the development of more efficient and powerful sources of EUV light. Such solid-state lasers may soon become a viable alternative given the fact that solid state lasers are more compact, are more flexible, and are expected to be more stable than presently used CO$_2$-gas lasers. Moreover, solid-state lasers are expected to have a significantly higher efficiency in converting electrical power to laser light, thus enabling obtaining a higher overall efficiency converting wall-plug electrical power to useful in-band EUV radiation. The optimum laser wavelength of such a solid-state drive laser, operating under realistic conditions, is however still unclear. At ARCNL, we are developing advanced high-energy, low-repetition rate laser systems [109], flexible in both wavelength (1-4 µm) and spatiotemporal beam profile. These laser systems will be employed to drive microdroplet tin plasma to produce EUV light under industrially relevant conditions, facilitating the design of the ultimate laser-driven plasma source of EUV light to drive tomorrow's nanolithography.

IV. CONCLUSIONS

In this topical review in the JOPT special issue on Advances in Optics in The Netherlands, key physics aspects of laser-driven tin plasmas are discussed. Such plasmas are the source of extreme ultraviolet light at 13.5-nm wavelength for state-of-the-art nanolithography. Generating ever-more EUV light at ever-increasing efficiencies and machine up-times provides a challenge to both science and industry. This is especially true in the context of a 1000 W EUV source, which now lies on the horizon of the semiconductor roadmap (such a source would quadruple the present source performance). In this review, we combine an overview of selected literature, focusing on recent results from the Advanced Research Center for Nanolithography (ARCNL) in Amsterdam. ARCNL is tasked to focus on the fundamental physics and chemistry underpinning current and future technologies for nanolithography. Progress towards, and beyond, a 1000 W EUV source will continue to be supported by achievements in the fields of optics and photonics field by combining fundamental research with industrial innovation.

ACKNOWLEDGMENTS

This work has been carried out at the Advanced Research Center for Nanolithography (ARCNL), a public-private partnership of the University of Amsterdam (UvA), the Vrije Universiteit Amsterdam, the Netherlands Organisation for Scientific Research (NWO) and the semiconductor equipment manufacturer ASML. The author gratefully acknowledges the team at ARCNL, comprising Dmitry Kurilovich, Francesco Torretti, Joris Scheers, Ruben Schupp, Lars Behnke, Yahia Mostafa, Bo Liu, Karl Schubert, Javier Hernandez-Rueda, Dion Engels, Maria Morbey, Jaap Hermens, Job Duffhues, Zoi Bouza, Alex Bayerle, Adam Lassise, Zeudi Mazzotta, Lucas Poirier, Diko Hemminga, Mart Johan Deuzeman, Subam Rai, Klaas Bijlsma, Laurens van Buuren, Randy Meijer, Tiago de Faria Pinto, and Kjeld Eikema. Further, input from Igor Fomenkov, Michael Purvis, Wim van der Zande, Fei Liu, Hanneke Gelderblom, Sten Reijers, Alexander Klein, James Byers Muharrem Bayraktar, Fred Bijkerk, Marcelo Ackermann, Alexander Windberger, Hendrik Bekker, José Crespo Lopez-Urrutia, Julian Berengut, Anastasia Borschevsky, Vivek Bakshi, Howard Scott, Amanda Neukirch, James Colgan, Alexandr Ryabtsev and Mikhail Basko (and many others) was much appreciated. This project has received funding from European Research Council (ERC) Starting Grant numbered 802648 and is part of the VIDI research programme with project number 15697, which is financed by the Netherlands Organisation for Scientific Research (NWO).

REFERENCES

---

[1] F. Torretti, J. Sheil, R. Schupp, M. M. Basko, M. Bayraktar, R. A. Meijer, S. Witte, W. Ubachs, R. Hoekstra, O. O. Versolato, A. J. Neukirch, and J. Colgan, Prominent radiative contributions from multiply-excited states in laser-produced tin plasma for nanolithography, Nat. Commun. **11**, 2334 (2020).

[2] C. A. Mack, Fifty Years of Moore's Law, IEEE Trans. Semicond. Manuf. **24**, 202 (2011).

[3] M. M. Waldrop, The chips are down for Moore's law, Nature **530**, 144 (2016).

[4] G. E. Moore, Cramming more components onto integrated circuits, Proc. IEEE **86**, 82 (1998).

[5] G. E. Moore, Progress in digital integrated electronics, Proc. IEDM Tech. Dig. **11**, 11 (1975).

[6] G. E. Moore, Lithography and the future of Moore's law, Proc. SPIE **2439**, 2439 (1995).

[7] J. van Schoot, K. Troost, F. Bornebroek, R. van Ballegoij, S. Lok, P. Krabbendam, J. Stoeldraijer, J. Benschop, J. Finders, H. Meiling, E. van Setten, B. Kneer, P. Kuerz, W. Kaiser, T. Heil, and S. Migura, The future of EUV lithography: continuing Moore's Law into the next decade, Proc. SPIE **10583**, 10.1117/12.2295800 (2018).

[8] S. Bajt, J. B. Alameda, T. W. Barbee, Jr., W. M. Clift, J. A. Folta, B. Kaufmann, and E. A. Spiller, Improved reflectance and stability of Mo-Si multilayers, Opt. Eng. **41**, 1797 (2002).

[9] Q. Huang, V. Medvedev, R. van de Kruijs, A. Yakshin, E. Louis, and F. Bijkerk, Spectral tailoring of nanoscale EUV and soft x-ray multilayer optics, Appl. Phys. Rev. **4**, 011104 (2017).

[10] R. A. Meijer, *Tailored Laser-Droplet Interaction: for Target Formation in Extreme Ultraviolet Sources*, Ph.D. thesis, Vrije Universiteit Amsterdam (2021).

[11] O. O. Versolato, Physics of laser-driven tin plasma sources of EUV radiation for nanolithography, Plasma Sources Sci. Technol. **28**, 083001 (2019).

[12] V. Bakshi, EUV sources for lithography (SPIE press Bellingham, Washington, 2006) Chap. 11.

[13] G. O'Sullivan, B. Li, R. D'Arcy, P. Dunne, P. Hayden, D. Kilbane, T. McCormack, H. Ohashi, F. O'Reilly, P. Sheridan, E. Sokell, C. Suzuki, and T. Higashiguchi, Spectroscopy of highly charged ions and its relevance to EUV and soft x-ray source development, J. Phys. B **48**, 144025 (2015).

[14] S. A. Reijers, D. Kurilovich, F. Torretti, H. Gelderblom, and O. O. Versolato, Laser-to-droplet alignment sensitivity relevant for laser-produced plasma sources of extreme ultraviolet light, J. Appl. Phys. **124**, 013102 (2018).

[15] D. Kurilovich, T. de Faria Pinto, F. Torretti, R. Schupp, J. Scheers, A. S. Stodolna, H. Gelderblom, K. S. Eikema, S. Witte, W. Ubachs, R. Hoekstra, and O. O. Versolato, Expansion Dynamics after Laser-Induced Cavitation in Liquid Tin Microdroplets, Phys. Rev. Appl. **10**, 054005 (2018).

[16] A. Vinokhodov, M. Krivokorytov, Y. Sidelnikov, V. Krivtsun, V. Medvedev, V. Bushuev, K. Koshelev, D. Glushkov, and S. Ellwi, Stable droplet generator for a high brightness laser produced plasma extreme ultraviolet source, Rev. Sci. Instrum. **87**, 103304 (2016).

[17] M. M. Basko, M. S. Krivokorytov, A. Y. Vinokhodov, Y. V. Sidelnikov, V. M. Krivtsun, V. V. Medvedev, D. A. Kim, V. O. Kompanets, A. A. Lash, and K. N. Koshelev, Fragmentation dynamics of liquid–metal droplets under ultra-short laser pulses, Laser Phys. Lett. **14**, 036001 (2017).

[18] M. S. Krivokorytov, A. Y. Vinokhodov, Y. V. Sidelnikov, V. M. Krivtsun, V. O. Kompanets, A. A. Lash,

K. N. Koshelev, and V. V. Medvedev, Cavitation and spallation in liquid metal droplets produced by subpicosecond pulsed laser radiation, Phys. Rev. E **95**, 031101 (2017).

[19] S. Y. Grigoryev, B. Lakatosh, M. Krivokorytov, V. Zhakhovsky, S. Dyachkov, D. Ilnitsky, K. Migdal, N. Inogamov, A. Y. Vinokhodov, V. Kompanets, *et al.*, Expansion and fragmentation of a liquid-metal droplet by a short laser pulse, Phys. Rev. Appl. **10**, 064009 (2018).

[20] P. Koukouvinis, N. Kyriazis, and M. Gavaises, Smoothed particle hydrodynamics simulation of a laser pulse impact onto a liquid metal droplet, PLoS One **13**, 1 (2018).

[21] T. de Faria Pinto, J. Mathijssen, R. Meijer, H. Zhang, A. Bayerle, D. Kurilovich, O. O. Versolato, K. S. Eikema, and S. Witte, Cylindrically and non-cylindrically symmetric expansion dynamics of tin microdroplets after ultrashort laser pulse impact, Appl. Phys. A **127**, 1 (2021).

[22] D. Kurilovich, A. L. Klein, F. Torretti, A. Lassise, R. Hoekstra, W. Ubachs, H. Gelderblom, and O. O. Versolato, Plasma propulsion of a metallic microdroplet and its deformation upon laser impact, Phys. Rev. Appl. **6**, 014018 (2016).

[23] D. Kurilovich, M. M. Basko, D. A. Kim, F. Torretti, R. Schupp, J. C. Visschers, J. Scheers, R. Hoekstra, W. Ubachs, and O. O. Versolato, Power-law scaling of plasma pressure on laser-ablated tin microdroplets, Phys. Plasmas **25**, 012709 (2018).

[24] D. Hudgins, N. Gambino, B. Rollinger, and R. Abhari, Neutral cluster debris dynamics in droplet-based laser-produced plasma sources, J. Phys. D **49**, 185205 (2016).

[25] A. L. Klein, W. Bouwhuis, C. W. Visser, H. Lhuissier, C. Sun, J. H. Snoeijer, E. Villermaux, D. Lohse, and H. Gelderblom, Drop shaping by laser-pulse impact, Phys. Rev. Appl. **3**, 044018 (2015).

[26] H. Gelderblom, H. Lhuissier, A. L. Klein, W. Bouwhuis, D. Lohse, E. Villermaux, and J. H. Snoeijer, Drop deformation by laser-pulse impact, J. Fluid Mech. **794**, 676 (2016).

[27] B. Liu, R. A. Meijer, J. Hernandez-Rueda, D. Kurilovich, Z. Mazzotta, S. Witte, and O. O. Versolato, Laser-induced vaporization of a stretching sheet of liquid tin, J. Appl. Phys. **129**, 053302 (2021).

[28] B. Liu, D. Kurilovich, H. Gelderblom, and O. O. Versolato, Mass loss from a stretching semitransparent sheet of liquid tin, Phys. Rev. Appl. **13**, 024035 (2020).

[29] A. Hassanein, T. Sizyuk, V. Sizyuk, and S. Harilal, Combined effects of pre-pulsing and target geometry on efficient EUV production from laser produced plasma experiments and modeling, in *Extreme Ultraviolet (EUV) Lithography II*, Vol. 7969, SPIE (International Society for Optics and Photonics, 2011) p. 79690D.

[30] J. Freeman, S. Harilal, and A. Hassanein, Enhancements of extreme ultraviolet emission using prepulsed Sn laser-produced plasmas for advanced lithography applications, J. Appl. Phys. **110**, 083303 (2011).

[31] J. R. Freeman, S. S. Harilal, A. Hassanein, and B. Rice, Effect of prepulse laser wavelength on EUV emission from CO_2 reheated laser-produced Sn plasma, Appl. Phys. A **110**, 853 (2013).

[32] M. Purvis, I. V. Fomenkov, A. A. Schafgans, M. Vargas, S. Rich, Y. Tao, S. I. Rokitski, M. Mulder, E. Buurman, M. Kats, J. Stewart, A. D. LaForge, C. Rajyaguru, G. Vaschenko, A. I. Ershov, R. J. Rafac, M. Abraham, D. C. Brandt, and D. J. Brown, Industrialization of a robust EUV source for high-volume manufacturing and power scaling beyond 250W, in *Extreme Ultraviolet (EUV) Lithography IX*, Vol. 10583 (SPIE, 2018) p. 1058327.

[33] S. Langer, H. Scott, T. Galvin, E. Link, B. Regan, and C. W. Siders, Simulations of Laser Driven EUV Sources – the Impact of Laser Wavelength, in *2020 Source Workshop* (EUV Litho, Inc., 2020) pp. 1 – 25.

[34] L. Behnke, R. Schupp, Z. Bouza, M. Bayraktar, Z. Mazzotta, R. Meijer, J. Sheil, S. Witte, W. Ubachs, R. Hoekstra, *et al.*, Extreme ultraviolet light from a tin plasma driven by a 2-μm-wavelength laser, Opt. Express **29**, 4475 (2021).

[35] J. Sheil, O. O. Versolato, H. Scott, and V. Bakshi, Review of the 1st EUV Source Code Comparison Workshop, in preparation (2021).

[36] EUV Litho, Inc., `https://euvlitho.com/`.

[37] K. Liu, Y. Li, F. Zhang, and M. Fan, Transient thermal and structural deformation and its impact on optical performance of projection optics for extreme ultraviolet lithography, Jpn. J. Appl. Phys. **46**, 6568 (2007).

[38] G. Yang and Y. Li, Analysis and control of thermal and structural deformation of projection optics for 22-nm EUV lithography, in *Extreme Ultraviolet (EUV) Lithography III*, Vol. 8322 (International Society for Optics and Photonics, 2012) p. 83222V.

[39] W. Svendsen and G. O'Sullivan, Statistics and characteristics of XUV transition arrays from laser-produced plasmas of the elements tin through iodine, Phys. Rev. A **50**, 3710 (1994).

[40] F. Torretti, R. Schupp, D. Kurilovich, A. Bayerle, J. Scheers, W. Ubachs, R. Hoekstra, and O. O. Versolato, Short-wavelength out-of-band EUV emission from Sn laser-produced plasma, J. Phys. B **51**, 045005 (2018).

[41] F. Torretti, F. Liu, M. Bayraktar, J. Scheers, Z. Bouza, W. Ubachs, R. Hoekstra, and O. Versolato, Spectral characterization of an industrial EUV light source for nanolithography, J. Phys. D **53**, 055204 (2019).

[42] J. Benschop, V. Banine, S. Lok, and E. Loopstra, Extreme ultraviolet lithography: Status and prospects, J. Vac. Sci. Technol. B **26**, 2204 (2008).

[43] V. Y. Banine, K. N. Koshelev, and G. H. P. M. Swinkels, Physical processes in EUV sources for microlithography, J. Phys. D: Appl. Phys. **44**, 253001 (2011).

[44] A. Z. Giovannini, N. Gambino, B. Rollinger, and R. S. Abhari, Angular ion species distribution in droplet-based laser-produced plasmas, J. Appl. Phys. **117**, 033302 (2015).

[45] M. J. Deuzeman, A. S. Stodolna, E. E. B. Leerssen, A. Antoncecchi, N. Spook, T. Kleijntjens, J. Versluis, S. Witte, K. S. E. Eikema, W. Ubachs, R. Hoekstra, and O. O. Versolato, Ion distribution and ablation depth measurements of a fs-ps laser-irradiated solid tin target, J. Appl. Phys. **121**, 103301 (2017).

[46] A. S. Stodolna, T. de Faria Pinto, F. Ali, A. Bayerle, D. Kurilovich, J. Mathijssen, R. Hoekstra, O. O. Versolato, K. S. E. Eikema, and S. Witte, Controlling ion kinetic energy distributions in laser produced plasma sources by means of a picosecond pulse pair, J. Appl.

Phys. **124**, 053303 (2018).

[47] A. Bayerle, M. J. Deuzeman, S. van der Heijden, D. Kurilovich, T. de Faria Pinto, A. Stodolna, S. Witte, K. S. E. Eikema, W. Ubachs, R. Hoekstra, and O. O. Versolato, Sn ion energy distributions of ns- and ps-laser produced plasmas, Plasma Sources Sci. Technol. **27**, 045001 (2018).

[48] M. M. Basko, V. G. Novikov, and A. S. Grushin, On the structure of quasi-stationary laser ablation fronts in strongly radiating plasmas, Phys. Plasmas **22**, 053111 (2015).

[49] J. Hernandez-Rueda, B. Liu, D. Hemminga, R. Meijer, D. Kurilovich, H. Gelderblom, J. Sheil, and O. O. Versolato, Early-time hydrodynamic response of a tin droplet impacted by laser-produced plasma, submitted (2021).

[50] G. Cisneros, J. S. Helman, and C. N. J. Wagner, Dielectric function of liquid tin between 250 and 1100°C, Phys. Rev. B **25**, 4248 (1982).

[51] F. E. C. Culick, Comments on a Ruptured Soap Film, J. Appl. Phys. **31**, 1128 (1960).

[52] R. A. Meijer, D. Kurilovich, B. Liu, Z. Mazzotta, J. Hernandez-Rueda, O. O. Versolato, and S. Witte, Laser ablation threshold of liquid tin microdroplets, submitted (2021).

[53] A. P. Shevelko, L. A. Shmaenok, S. S. Churilov, R. K. F. J. Bastiaensen, and F. Bijkerk, Extreme Ultraviolet Spectroscopy of a Laser Plasma Source for Lithography, Phys. Scr. **57**, 276 (1998).

[54] R. L. Kauffman, D. W. Phillion, and R. C. Spitzer, X-ray production ∼13 nm from laser-produced plasmas for projection x-ray lithography applications, Appl. Opt. **32**, 6897 (1993).

[55] P. Hayden, A. Cummings, N. Murphy, G. O'Sullivan, P. Sheridan, J. White, and P. Dunne, 13.5 nm extreme ultraviolet emission from tin based laser produced plasma sources, J. Appl. Phys. **99**, 093302 (2006).

[56] S. S. Harilal, B. O. Shay, M. S. Tillack, Y. Tao, R. Paguio, A. Nikroo, and C. A. Back, Spectral control of emissions from tin doped targets for extreme ultraviolet lithography, J. Appl. Phys. **39**, 484 (2006).

[57] Y. Tao, S. Harilal, M. Tillack, K. Sequoia, B. O'Shay, and F. Najmabadi, Effect of focal spot size on in-band 13.5 nm extreme ultraviolet emission from laser-produced Sn plasma, Opt. Lett. **31**, 2492 (2006).

[58] R. W. Coons, S. S. Harilal, D. Campos, and A. Hassanein, Analysis of atomic and ion debris features of laser-produced Sn and Li plasmas, J. Appl. Phys. **108**, 063306 (2010).

[59] D. Campos, S. Harilal, and A. Hassanein, The effect of laser wavelength on emission and particle dynamics of Sn plasma, J. Appl. Phys. **108**, 113305 (2010).

[60] S. A. George, W. T. Silfvast, K. Takenoshita, R. T. Bernath, C.-S. Koay, G. Shimkaveg, and M. C. Richardson, Comparative extreme ultraviolet emission measurements for lithium and tin laser plasmas, Opt. Lett. **32**, 997 (2007).

[61] R. Schupp, F. Torretti, R. Meijer, M. Bayraktar, J. Scheers, D. Kurilovich, A. Bayerle, K. Eikema, S. Witte, W. Ubachs, R. Hoekstra, and O. O. Versolato, Efficient Generation of Extreme Ultraviolet Light From Nd:YAG-Driven Microdroplet-Tin Plasma, Phys. Rev. Appl. **12**, 014010 (2019).

[62] Y. Shimada, H. Nishimura, M. Nakai, K. Hashimoto, M. Yamaura, Y. Tao, K. Shigemori, T. Okuno, K. Nishihara, T. Kawamura, A. Sunahara, T. Nishikawa, A. Sasaki, K. Nagai, T. Norimatsu, S. Fujioka, S. Uchida, N. Miyanaga, Y. Izawa, and C. Yamanaka, Characterization of extreme ultraviolet emission from laser-produced spherical tin plasma generated with multiple laser beams, Appl. Phys. Lett, **86**, 051501 (2005).

[63] H. Tanaka, A. Matsumoto, K. Akinaga, A. Takahashi, and T. Okada, Comparative study on emission characteristics of extreme ultraviolet radiation from CO_2 and Nd:YAG laser-produced tin plasmas, Appl. Phys. Lett. **87**, 041503 (2005).

[64] S. S. Harilal, R. W. Coons, P. Hough, and A. Hassanein, Influence of spot size on extreme ultraviolet efficiency of laser-produced Sn plasmas, Appl. Phys. Lett. **95**, 221501 (2009).

[65] S. Harilal, T. Sizyuk, A. Hassanein, D. Campos, P. Hough, and V. Sizyuk, The effect of excitation wavelength on dynamics of laser-produced tin plasma, J. Appl. Phys. **109**, 063306 (2011).

[66] Y. Ueno, G. Soumagne, A. Sumitani, A. Endo, and T. Higashiguchi, Enhancement of extreme ultraviolet emission from a CO_2 laser-produced Sn plasma using a cavity target, Appl. Phys. Lett. **91**, 231501 (2007).

[67] R. Amano, T.-H. Dinh, A. Sasanuma, G. Arai, H. Hara, Y. Fujii, T. Hatano, T. Ejima, W. Jiang, A. Sunahara, A. Takahashi, D. Nakamura, T. Okada, K. Sakaue, T. Miura, G. O'Sullivan, and T. Higashiguchi, Influence of short pulse duration of carbon dioxide lasers on extreme ultraviolet emission from laser-produced plasmas, Jpn. J. Appl. Phys. **57**, 070311 (2018).

[68] M. Yamaura, S. Uchida, A. Sunahara, Y. Shimada, H. Nishimura, S. Fujioka, T. Okuno, K. Hashimoto, K. Nagai, T. Norimatsu, K. Nishihara, N. Miyanga, Y. Izawa, and C. Yamanaka, Characterization of extreme ultraviolet emission using the fourth harmonic of a Nd:YAG laser, Appl. Phys. Lett. **86**, 181107 (2005).

[69] H. Mizoguchi, H. Nakarai, T. Abe, H. Tanaka, Y. Watanabe, T. Hori, Y. Shiraishi, T. Yanagida, G. Soumagne, T. Yamada, and T. Saitou, Challenge of $>$ 300W high power LPP-EUV source with long collector mirror lifetime for semiconductor HVM, in *Extreme Ultraviolet (EUV) Lithography XI*, Vol. 11323 (SPIE, 2020) pp. 225 – 238.

[70] I. Fomenkov, D. Brandt, A. Ershov, A. Schafgans, Y. Tao, G. Vaschenko, S. Rokitski, M. Kats, M. Vargas, M. Purvis, R. Rafac, B. L. Fontaine, S. D. Dea, A. LaForge, J. Stewart, S. Chang, M. Graham, D. Riggs, T. Taylor, M. Abraham, and D. Brown, Light sources for high-volume manufacturing EUV lithography: technology, performance, and power scaling, Adv. Opt. Techn. **6**, 173 (2017).

[71] J. R. Freeman, S. S. Harilal, B. Verhoff, A. Hassanein, and B. Rice, Laser wavelength dependence on angular emission dynamics of Nd:YAG laser-produced Sn plasmas, Plasma Sources Sci. Technol. **21**, 055003 (2012).

[72] R. Schupp, L. Behnke, J. Sheil, Z. Bouza, M. Bayraktar, W. Ubachs, R. Hoekstra, and O. O. Versolato, Characterization of 1-and 2- μ m-wavelength laser-produced microdroplet-tin plasma for generating extreme-ultraviolet light, Phys. Rev. Res. **3**, 013294 (2021).

[73] V. Bakshi, ed., *EUV Lithography*, 2nd Edition ed. (SPIE Press, 2018).

[74] C. W. Siders, A. C. Erlandson, T. C. Galvin, H. Frank, S. Langer, B. A. Reagan, H. Scott, E. F. Sistrunk, and T. M. Spinka, Efficient high power laser drivers for next-generation High Power EUV sources, in *2019 Source Workshop* (EUV Litho, Inc., 2019) pp. 1–23.

[75] R. Schupp, F. Torretti, R. A. Meijer, M. Bayraktar, J. Sheil, J. Scheers, D. Kurilovich, A. Bayerle, A. A. Schafgans, M. Purvis, K. S. E. Eikema, S. Witte, W. Ubachs, R. Hoekstra, and O. O. Versolato, Radiation transport and scaling of optical depth in Nd:YAG laser-produced microdroplet-tin plasma, Appl. Phys. Lett. **115**, 124101 (2019).

[76] S. Fujioka, H. Nishimura, K. Nishihara, A. Sasaki, A. Sunahara, T. Okuno, N. Ueda, T. Ando, Y. Tao, Y. Shimada, K. Hashimoto, M. Yamaura, K. Shigemori, M. Nakai, K. Nagai, T. Norimatsu, T. Nishikawa, N. Miyanaga, Y. Izawa, and K. Mima, Opacity Effect on Extreme Ultraviolet Radiation from Laser-Produced Tin Plasmas, Phys. Rev. Lett. **95**, 235004 (2005).

[77] J. White, P. Dunne, P. Hayden, F. O'Reilly, and G. O'Sullivan, Optimizing 13.5 nm laser-produced tin plasma emission as a function of laser wavelength, Appl. Phys. Lett. **90**, 181502 (2007).

[78] R. Schupp, L. Behnke, Z. Bouza, Z. Mazzotta, Y. Mostafa, A. Lassise, L. Poirier, J. Sheil, M. Bayraktar, W. Ubachs, *et al.*, Characterization of angularly resolved EUV emission from 2-μm-wavelength laser-driven Sn plasmas using preformed liquid disk targets, J. Phys. D **54** (2021).

[79] C. Wagner and N. Harned, Lithography gets extreme, Nat. Photonics **4**, 24 (2010).

[80] Y. Kawasuji, K. M. Nowak, T. Hori, T. Okamoto, H. Tanaka, Y. Watanabe, T. Abe, T. Kodama, Y. Shiraishi, H. Nakarai, *et al.*, Key components technology update of the 250W high-power LPP-EUV light source, in *SPIE Advanced Lithography*, Vol. 10143 (International Society for Optics and Photonics, 2017) pp. 101432G–101432G.

[81] V. I. Azarov and Y. N. Joshi, Analysis of the 4d^7-4d^{6}5p transition array of the eighth spectrum of tin: Sn VIII, J. Phys. B **26**, 3495 (1993).

[82] S. S. Churilov and A. N. Ryabtsev, Analyses of the Sn IX–Sn XII spectra in the EUV region, Phys. Scr. **73**, 614 (2006).

[83] S. S. Churilov and A. N. Ryabtsev, Analysis of the 4p 64d 7-(4p 64d 64f+ 4p 54d 8) transitions in the Sn VIII spectrum, Opt. Spectrosc. **100**, 660 (2006).

[84] S. S. Churilov and A. N. Ryabtsev, Analysis of the spectra of In XII–XIV and Sn XIII–XV in the far-VUV region, Opt. Spectrosc. **101**, 169 (2006).

[85] A. N. Ryabtsev, É. Y. Kononov, and S. S. Churilov, Spectra of rubidium-like Pd X-Sn XIV ions, Opt. Spectrosc. **105**, 844 (2008).

[86] I. Y. Tolstikhina, S. S. Churilov, A. N. Ryabtsev, and K. N. Koshelev, Atomic tin data, in *EUV sources for lithography*, edited by V. Bakshi (SPIE Press, 2006) Chap. 4, pp. 113–148.

[87] H. Ohashi, S. Suda, H. Tanuma, S. Fujioka, H. Nishimura, A. Sasaki, and K. Nishihara, EUV emission spectra in collisions of multiply charged Sn ions with He and Xe, J. Phys. B **43**, 065204 (2010).

[88] A. Windberger, F. Torretti, A. Borschevsky, A. Ryabtsev, S. Dobrodey, H. Bekker, E. Eliav, U. Kaldor, W. Ubachs, R. Hoekstra, J. R. Crespo López-Urrutia, and O. O. Versolato, Analysis of the fine structure of Sn^{11+}–Sn^{14+} ions by optical spectroscopy in an electron-beam ion trap, Phys. Rev. A **94**, 012506 (2016).

[89] J. Colgan, D. Kilcrease, J. Abdallah, M. Sherrill, C. Fontes, P. Hakel, and G. Armstrong, Atomic structure considerations for the low-temperature opacity of Sn, High Energy Density Phys. **23**, 133 (2017).

[90] F. Torretti, A. Windberger, A. Ryabtsev, S. Dobrodey, H. Bekker, W. Ubachs, R. Hoekstra, E. V. Kahl, J. C. Berengut, J. R. C. López-Urrutia, and O. O. Versolato, Optical spectroscopy of complex open-4d-shell ions Sn^{7+} − Sn^{10+}, Phys. Rev. A **95**, 042503 (2017).

[91] J. Bauche, C. Bauche-Arnoult, and M. Klapisch, Transition arrays in the spectra of ionized atoms, Adv. Atom. Mol. Phys. **23**, 131 (1988).

[92] J. Sheil, O. O. Versolato, A. J. Neukirch, and J. Colgan, Multiply-excited states and their contribution to opacity in CO$_2$ laser-driven tin-plasma conditions, J. Phys. B **54**, 035002 (2021).

[93] M. Busquet, Radiation-dependent ionization model for laser-created plasmas, Phys. Fluids B **5**, 4191 (1993).

[94] J. Scheers, C. Shah, A. Ryabtsev, H. Bekker, F. Torretti, J. Sheil, D. A. Czapski, J. C. Berengut, W. Ubachs, J. R. C. López-Urrutia, R. Hoekstra, and O. O. Versolato, EUV spectroscopy of highly charged Sn^{13+} − Sn^{15+} ions in an electron-beam ion trap, Phys. Rev. A **101**, 062511 (2020).

[95] Z. Bouza, J. Scheers, A. Ryabtsev, R. Schupp, L. Behnke, C. Shah, J. Sheil, M. Bayraktar, J. R. C. López-Urrutia, W. Ubachs, R. Hoekstra, and O. O. Versolato, EUV spectroscopy of Sn^{5+}–Sn^{10+} ions in an electron beam ion trap and laser-produced plasmas, J. Phys. B **53**, 195001 (2020).

[96] Z. Bouza, J. Byers, J. Scheers, R. Schupp, Y. Mostafa, L. Behnke, Z. Mazzotta, J. Sheil, W. Ubachs, R. Hoekstra, M. Bayraktar, and O. O. Versolato, The spectrum of a 1-μm-wavelength-driven tin microdroplet laser-produced plasma source in the 5.5–265.5 nm wavelength range, AIP Adv. **11**, 125003 (2021).

[97] J. Byers, Z. Bouza, O. O. Versolato, and M. Bayraktar, Imaging transmission grating spectrometer using a tapered fresnel zone plate, in preparation (2022).

[98] J. Scheers, A. Ryabtsev, A. Borschevsky, J. C. Berengut, K. Haris, R. Schupp, D. Kurilovich, F. Torretti, A. Bayerle, E. Eliav, *et al.*, Energy-level structure of Sn^{3+} ions, Phys. Rev. A **98**, 062503 (2018).

[99] J. Scheers, R. Schupp, R. Meijer, W. Ubachs, R. Hoekstra, and O. O. Versolato, Time-and space-resolved optical Stark spectroscopy in the afterglow of laser-produced tin-droplet plasma, Phys. Rev. E **102**, 013204 (2020).

[100] S. Rai, K. Bijlsma, S. Koeleman, O. Tjepkema, A. Noordam, H. Jonkman, O. Versolato, and R. Hoekstra, Single-collision scattering of keV-energy Kr ions off a polycrystalline Cu surface, Nucl. Instrum. Methods Phys. Res. B **482**, 58 (2020).

[101] S. Rai, M. Deuzemann, W. Noordam, E. Holleman, O. O. Versolato, and R. Hoekstra, The missing single-scattering peak in tin ion collisions on Mo and Ru targets, in *J. Phys. Conf. Ser.*, Vol. 1412 (IOP Publishing, 2020) p. 202019.

[102] J. Ziegler, J. Biersack, and U. Littmark, The Stopping and Range of Ions in Matter, in *Treatise on heavy-ion science* (Pergamon Press, New York, 1985) pp. 93–129.

[103] R. Hoekstra, F. J. De Heer, and R. Morgenstern, State-selective electron capture in collisions of He^{2+} with H, J. Phys. B **24**, 4025 (1991).

[104] H. O. Folkerts, F. W. Bliek, M. C. De Jong, R. Hoekstra, and R. Morgenstern, Dissociation of CO induced by ions: I. Fragmentation and kinetic energy release spectra, J. Phys. B **30**, 5833 (1997).

[105] P. Mora, Plasma expansion into a vacuum, Phys. Rev. Lett. **90**, 185002 (2003).

[106] D. J. Hemminga, L. Poirier, M. M. Basko, R. Hoekstra, W. Ubachs, O. O. Versolato, and J. Sheil, High-energy ions from Nd: YAG laser ablation of tin microdroplets: comparison between experiment and a single-fluid hydrodynamic model, Plasma Sources Sci. Technol. **30**, 105006 (2021).

[107] L. Poirier, W. Ubachs, O. Versolato, J. Sheil, and R. Hoekstra, Cross-calibration of a combined electrostatic and time-of-flight analyzer for energy- and charge-state-resolved spectrometry of tin laser-produced plasma, accepted (2021).

[108] M. van de Kerkhof, F. Liu, M. Meeuwissen, X. Zhang, M. Bayraktar, R. de Kruif, and N. Davydova, High-power EUV lithography: spectral purity and imaging performance, J. Micro Nanolithogr. MEMS MOEMS **19**, 033801 (2020).

[109] Z. Mazzotta, J. Mathijssen, K. Eikema, O. Versolato, and S. Witte, TI-REX: A Tunable Infrared laser for Experiments in nanolithography, in *The European Conference on Lasers and Electro-Optics* (Optical Society of America, 2021) p. cd_p_28.